



**HAL**  
open science

## **SARS-CoV-2 E and 3a proteins are inducers of pannexin currents**

Barbara Oliveira Mendes, Malak Alameh, Beatrice Ollivier, Jérôme Montnach, Nicolas Bidère, Frederique Souaze, Nicolas Escriou, Flavien Charpentier, Isabelle Baro, Michel de Waard, et al.

► **To cite this version:**

Barbara Oliveira Mendes, Malak Alameh, Beatrice Ollivier, Jérôme Montnach, Nicolas Bidère, et al.. SARS-CoV-2 E and 3a proteins are inducers of pannexin currents. 2022. hal-04234657v1

**HAL Id: hal-04234657**

**<https://nantes-universite.hal.science/hal-04234657v1>**

Preprint submitted on 21 Oct 2022 (v1), last revised 10 Oct 2023 (v2)

**HAL** is a multi-disciplinary open access archive for the deposit and dissemination of scientific research documents, whether they are published or not. The documents may come from teaching and research institutions in France or abroad, or from public or private research centers.

L'archive ouverte pluridisciplinaire **HAL**, est destinée au dépôt et à la diffusion de documents scientifiques de niveau recherche, publiés ou non, émanant des établissements d'enseignement et de recherche français ou étrangers, des laboratoires publics ou privés.



Distributed under a Creative Commons Attribution - NonCommercial - NoDerivatives 4.0 International License

1 **SARS-CoV-2 E and 3a proteins are inducers of pannexin currents**

2

3

4

5 Barbara Oliveira Mendes<sup>1,#</sup>, Malak Alameh<sup>1,2,#</sup>, Béatrice Ollivier<sup>1</sup>, Jérôme Montnach<sup>1</sup>, Nicolas  
6 Bidère<sup>3,4</sup>, Frédérique Souazé<sup>5</sup>, Nicolas Escriou<sup>6</sup>, Flavien Charpentier<sup>1</sup>, Isabelle Baró<sup>1</sup>, Michel  
7 De Waard<sup>1,2,§,\*</sup>, Gildas Loussouarn<sup>1,§,\*</sup>

8

9 <sup>1</sup>Nantes Université, CNRS, INSERM, l'institut du thorax, Nantes, France

10 <sup>2</sup>Labex Ion Channels, Science and Therapeutics, Valbonne, France

11 <sup>3</sup>Team SOAP, CRCI2NA, Nantes Université, Inserm, CNRS, Université d'Angers, Nantes,  
12 France

13 <sup>4</sup>Equipe Labellisée Ligue Contre le Cancer, Paris, France

14 <sup>5</sup>Nantes Université, INSERM, CNRS, CRCI2NA, Nantes, France

15 <sup>6</sup>Institut Pasteur, Université Paris Cité, Département de Santé Globale, Paris, France

16

17 # these authors contributed equally to this work.

18 § Both senior authors codirected this work.

19

20 \* Corresponding authors: [michel.dewaard@univ-nantes.fr](mailto:michel.dewaard@univ-nantes.fr) or  
21 [gildas.loussouarn@univ-nantes.fr](mailto:gildas.loussouarn@univ-nantes.fr); Tel.: +33-228-080-076

22

23 **Short title:** Ionic conductances triggered by SARS-CoV-2 E and 3a proteins

## 24 **Abstract**

25

26 Controversial reports have suggested that SARS-CoV E and 3a proteins may be viroporins that  
27 conduct currents through the plasma membrane of the infected cells. If true, these proteins  
28 would represent accessible targets for the development of new antiviral drugs by using high-  
29 throughput patch-clamp techniques. Here we aimed at better characterizing the cell responses  
30 induced by E or 3a protein with a particular focus on the ion conductances measured at the cell  
31 surface. First, we show that expression of SARS-CoV-2 E or 3a protein in CHO cells gives rise to  
32 cells with newly-acquired round shape, tending to detach from the Petri dish. This suggests that  
33 cell death is induced upon expression of E or 3a protein. We confirmed this hypothesis by using  
34 flow cytometry, in agreement with earlier reports on other cell types. In adhering cells  
35 expressing E or 3a protein, whole-cell currents were in fact not different from the control  
36 condition indicating that E and 3a proteins are not plasma membrane viroporins. In contrast,  
37 recording currents on detached cells uncovered outwardly-rectifying currents, much larger than  
38 those observed in control. The current characteristics are reminiscent of what was previously  
39 observed in cells expressing SARS-CoV-1 E or 3a proteins. Herein, we illustrate for the first time  
40 that carbenoxolone blocks these outward currents suggesting that they are conducted by  
41 pannexin channels, mostly likely activated by cell morphology change and/or cell death.  
42 Alongside we also demonstrate that truncation of the C-terminal PDZ binding motifs reduces the  
43 proportion of dying cells but does not prevent pannexin currents suggesting distinct pathways  
44 for cell death and pannexin currents induced by E and 3a proteins. We conclude that SARS-CoV-  
45 2 E and 3a proteins are not acting as viroporins expressed at the plasma membrane.

46

## 47 **Author Summary**

48

49 A viroporin (or viral porin) is a class of proteins that is encoded by a virus genome. It is named  
50 porin because its biological role is to conduct ions through a pore that it created in a lipid  
51 membrane such as the one surrounding a human cell. If such viroporin is present at the external  
52 membrane of a human cell infected by a virus, it can be an easy target of an antiviral agent which  
53 thus does not have to enter the cell to be active. One example of viroporin is the flu M2 protein  
54 that is the target of amantadine, an antiviral agent used against flu. In previous studies, two  
55 proteins of SARS-CoV viruses, named E protein and 3a protein, have been suggested to be  
56 viroporins at the surface of infected human cells, potentially opening a new research avenue  
57 against SARS. Here we demonstrate that both proteins are not viroporins at the external  
58 membrane but they rather trigger changes in the cell shape and promote cell death. They only  
59 indirectly induce the activity of a porin that is encoded by the cell genome, named pannexin.

## 60 Introduction

61

62 SARS-CoV-2 is the third virus of the genus Beta-coronavirus of the Coronaviridae family to be  
63 responsible for a Severe Acute Respiratory Syndrome in this century, after SARS-CoV-1 in 2002-  
64 2003 (1) and MERS-CoV in 2012 (2). As a result, it is of great importance to best characterize  
65 coronaviruses and the associated pathophysiology, with the hope that new treatments will  
66 emerge to complement vaccine approaches for people who cannot access the vaccines or are  
67 not responsive to them. In addition to paxlovid which is already available but associated with  
68 bothersome side-effects (3), many potential anti-COVID-19 treatments are in development but  
69 it is too soon to tell how efficient they will be, namely with regard to the continuous emergence  
70 of new variants, and if the cost will be reasonable (4).

71 Viroporins, *i.e.* ion channels encoded by a virus genome, are potential targets by antiviral agents,  
72 as demonstrated by the case of amantadine which inhibits the acid-activated M2 channel of  
73 Influenza A virus (5). Several studies led to the suggestion that two proteins of SARS-CoV are  
74 viroporins. SARS-CoV-2 Envelop (E) protein, is a one-transmembrane-domain membrane protein  
75 (75 amino-acids) almost identical to SARS-CoV-1 Envelop protein (95% identity). The SARS-CoV-  
76 2 ORF3a (3a) protein is a larger three-transmembrane-domain membrane protein (275 amino-  
77 acids) relatively similar to the SARS-CoV-1 3a protein (73% identity).

78 Regarding the ion channel function of these proteins, there are clearly several contradicting  
79 studies: some of them raising intriguing issues and others not confirming these reports.  
80 Concerning *in-vitro* membrane incorporation of purified E or 3a protein in lipid bilayers, the  
81 presence of ion channel activity was reportedly associated with these viral proteins (6–11).  
82 However, a review article soundly outlined the lack of robust data and raised ethical concerns  
83 casting doubts on the validity of the scientific messages (12). Concerning viral protein expression  
84 in cells, the expression of SARS-CoV-1 E protein also led to conflicting results (13,14). Pervushin  
85 et al managed to identify plasma membrane currents generated by heterologous expression of  
86 SARS-CoV-1 E protein in HEK-293 cells (13) but not Nieto-Torres et al (14). More recently,  
87 expression of wild-type (WT) SARS-CoV-2 E protein did not lead to interpretable ionic currents  
88 in HEK-293S or *Xenopus laevis* oocytes (15) despite their high homology among SARS-CoV  
89 viruses. In an attempt to favor plasma membrane targeting and reveal a putative current, a C-  
90 terminal predicted ER retention signal of SARS-CoV-1 E protein was replaced by a Golgi export  
91 signal from Kir2.1 channel. Expression of this chimera could then be associated with the  
92 generation of a non-rectifying and cation-selective current. This current was thus quite different  
93 from the outwardly rectifying current observed by Pervushin and collaborators (15).  
94 Furthermore, another study using a membrane targeting sequence, fused to the N-terminus of  
95 the SARS-CoV-1 E protein, provided a non-rectifying current that was 100-fold larger than the  
96 one observed in the two previous studies (16). This suggests that such modification of either N-  
97 or C-terminus are too drastic to faithfully report the actual activity of the native proteins.

98 SARS-CoV-1 3a protein was also investigated and expression of the WT protein in HEK-293 cells  
99 (17) or *Xenopus laevis* oocytes (18–20) was associated with a poorly selective outwardly  
100 rectifying current in both models, resembling to the one observed upon expression of the E  
101 protein.

102 To summarize, there is no unequivocal evidence that SARS-CoV E and 3a proteins are viroporins  
103 active at the plasma membrane of the host cell. However, it was recently reported that SARS-

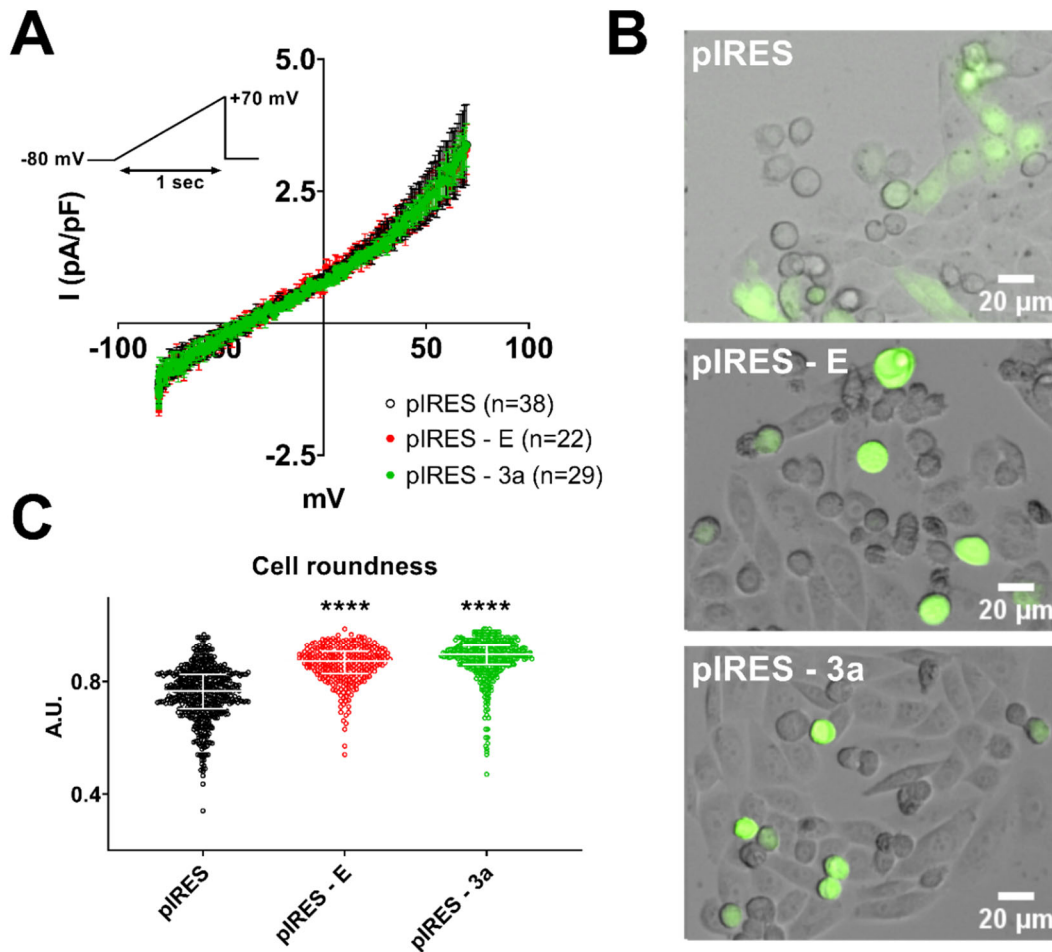
104 CoV-2 E and 3a proteins can promote cell death (21,22), on one hand. On the other hand,  
105 apoptosis is associated with the increase of an outwardly-rectifying current conducted by  
106 pannexins (23–25). This led us to reinvestigate the actual function(s) of SARS-CoV-2 E and 3a  
107 proteins in mammalian cells in the frame of the cell toxicity of these proteins.

108 In this study, CHO cells expressing either CoV-2 E or 3a proteins tended to develop into a round-  
109 shaped form with a tendency to detach from the Petri dish, a process exacerbated compared to  
110 control conditions. This cell phenotype is consistent with cell death (26,27) and we confirmed  
111 by flow cytometry experiments that expression of E or 3a proteins does indeed promote cell  
112 death. Transfected cells, still attached to the Petri dish (adhering cells), had unchanged basal  
113 currents indicating that E and 3a proteins are unlikely to act as plasma membrane channels. In  
114 contrast, recording whole-cell currents on round-shaped and detached cells, we observed large  
115 outwardly-rectifying currents only in E or 3a protein-expressing cells but not in control dying  
116 cells. This current is reminiscent of those observed in previous publications using HEK-293 cells  
117 and oocytes expressing the SARS-CoV-1 proteins (13,18–20). Application of carbenoxolone, a  
118 pannexin channel inhibitor, suggests for the first time that these currents are pannexin-  
119 mediated conductances, potentially activated in apoptotic cells. In conclusion, both SARS-CoV-2  
120 E and 3a proteins are most likely triggers of endogenous conductance.

121

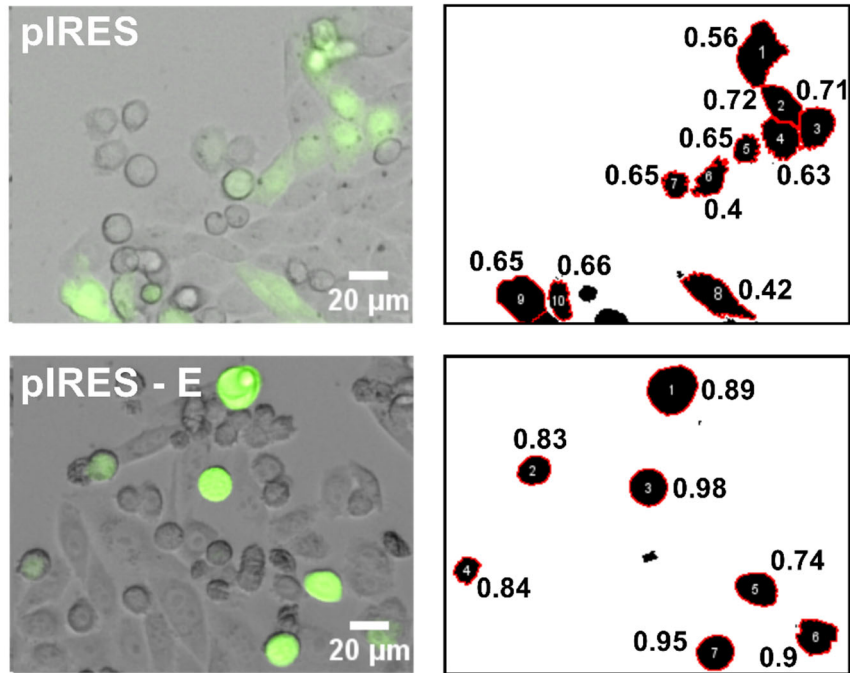
## 122 **Results**

123 We first focused on native E and 3a proteins. To maximize the chance of observing E and 3a  
124 protein-induced ionic currents, we chose to use pIRES plasmids, in which the protein of interest  
125 situated in the first cassette is more expressed than the eGFP reporter in the second cassette,  
126 thereby guaranteeing expression of a high level of the protein of interest in fluorescent cells  
127 (28,29). For the purpose of this study, we also selected CHO rather than HEK-293 cells because  
128 they express minimal endogenous currents (30). We compared whole-cell currents recorded  
129 during a ramp protocol, in cells transfected either with a control pIRES2-eGFP plasmid (pIRES),  
130 or the same plasmid containing the cDNA of the SARS-CoV-2 E protein (pIRES - E) or 3a protein  
131 (pIRES - 3a). Unexpectedly, we did not observe any difference in the currents recorded for the  
132 SARS-CoV-2 proteins expressing cells compared to control pIRES condition (Figure 1A). However,  
133 many cells transfected with either E- or 3a-encoding plasmids were developing altered  
134 morphology, shifting from spindle-like cells to more round cells (Figure 1B), similar to what was  
135 previously observed in MDCK cells heterologously expressing SARS-CoV-1 E protein (31).  
136 Analysis with Fiji tool confirmed an increase in cell roundness (Figure 1C and suppl. Figure 1). In  
137 particular, in patch-clamp experiments, some cells were coming off from the dish bottom by  
138 losing adhesion. Cell counting indicated that slightly more cells were losing adhesion when E or  
139 3a protein were expressed ( $3.4 \pm 0.6$  % in non-transfected cells,  $5.2 \pm 1.0$ % in pIRES condition,  
140  $6.6 \pm 0.7$ % in pIRES - E,  $6.0 \pm 1.2$ % in pIRES - 3a, n=3-5). As classically performed, currents shown  
141 in Figure 1A were recorded from adhering cells while non-adhering cells were disregarded in this  
142 initial investigation. Noteworthy, in each condition, both spindle-like and round adhering cells  
143 were studied (pIRES: 21 spindle-like and 17 round cells; pIRES E: 9 and 13, pIRES 3a: 18 and 11).

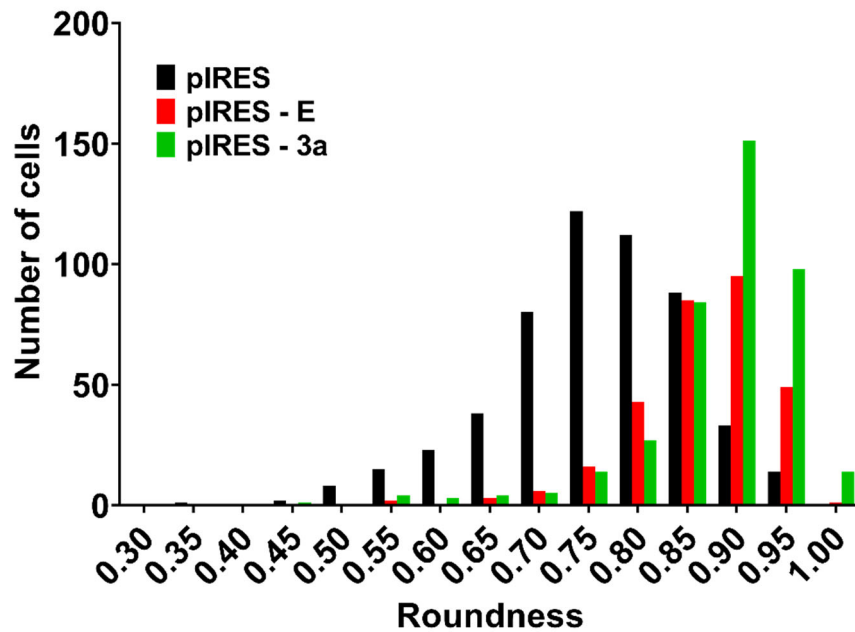


144  
 145 **Figure 1: Expression of E and 3a protein is accompanied by altered cellular morphology but no**  
 146 **modification in whole-cell currents in adhering cells. (A)** Average current densities ( $\pm$  sem)  
 147 recorded during the ramp protocol (inset) in adhering CHO cells expressing either eGFP (pIRES),  
 148 SARS-CoV-2 E and eGFP proteins (pIRES - E) or SARS-CoV-2 3a and eGFP proteins (pIRES - 3a). **(B)**  
 149 Superimposed brightfield and eGFP fluorescence images of CHO cells in the same 3 conditions  
 150 as shown in A. **(C)** Analysis of cell roundness in cell automatically detected by Fiji, cf. suppl. Figure  
 151 1. Plot of individual cells (pIRES, n = 1922; pIRES - E, n = 1198; and pIRES - 3a, n = 1283), median  
 152  $\pm$  interquartile range. \*\*\*\* p < 0.0001 as compared to pIRES control, Kruskal-Wallis test.

**A**



**B**



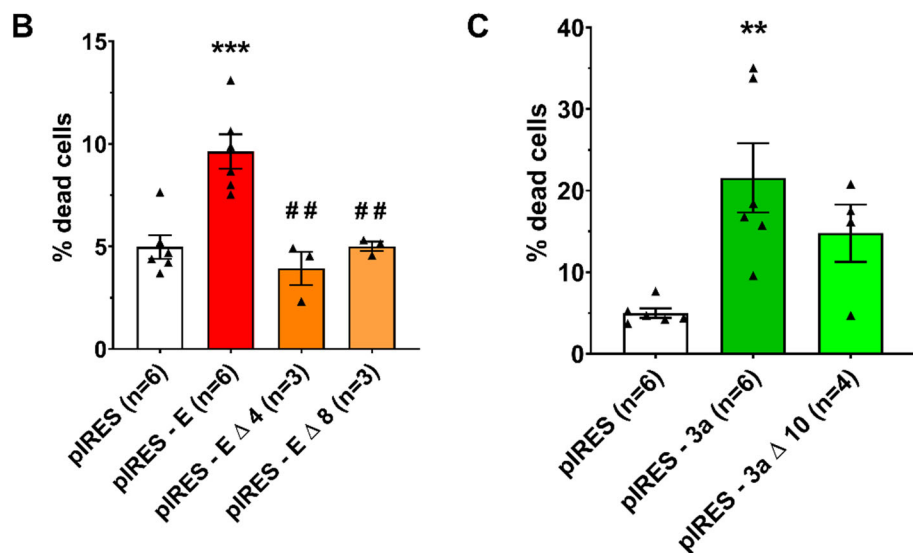
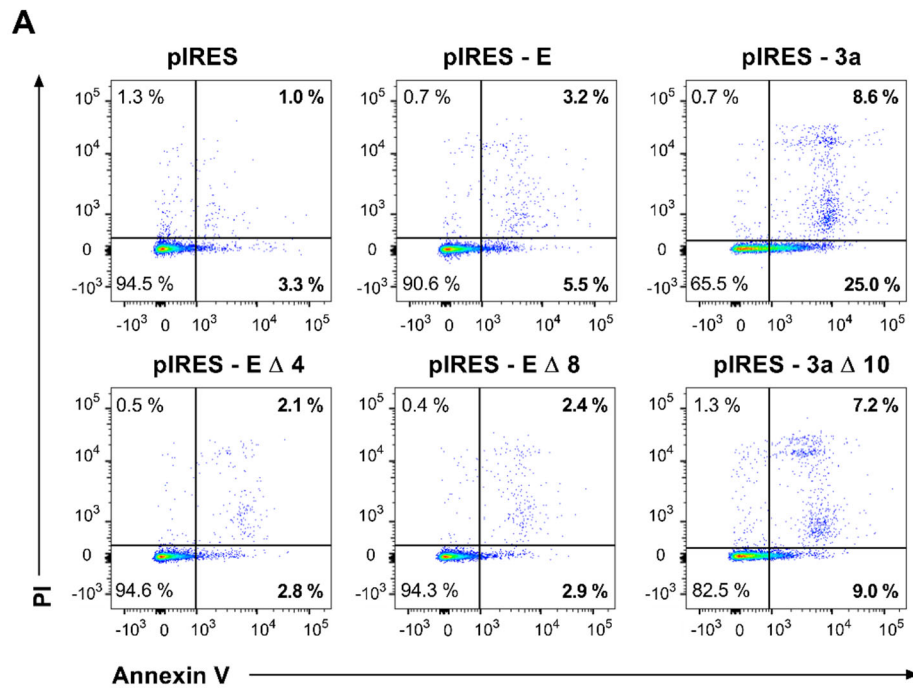
153

154 **Suppl. Figure 1: Morphology analysis of cells transfected with control pIRES or pIRES - E**  
 155 **plasmids. (A)** Left: example of superimposed brightfield and eGFP fluorescence images. Right:  
 156 Automatic particle analysis showing the roundness index **(B)** Distribution of cells roundnesses  
 157 from the analysis of 5 areas of 1.7 mm x 1.7 mm for cells transfected with control pIRES, pIRES -  
 158 E or pIRES- 3a plasmids.

159 Since both E and 3a proteins are promoting cell death (21,22), we hypothesized that the various  
160 cell morphological patterns (spindle-shaped, round-adhering, and round non-adhering) may  
161 correspond to the development of cell death, as described earlier in CHO and other cells (26,27).  
162 Flow cytometry analysis performed on the eGFP-positive CHO cells (Figure 2) showed that  
163 expression of E and 3a proteins increases the percentage of dying cells, more significantly late  
164 cell death, revealed by propidium iodide permeability (suppl. Figure 2). The effect of 3a protein  
165 was greater than the effect of the E protein. E protein-induced cell death could be reduced by  
166 the pan-caspase inhibitor QVD-Oph, while 3a protein-induced cell death was not (suppl. Figures  
167 3 & 4), suggesting that E protein induces apoptosis, while 3a protein activates non-conventional  
168 caspase-independent cell death.

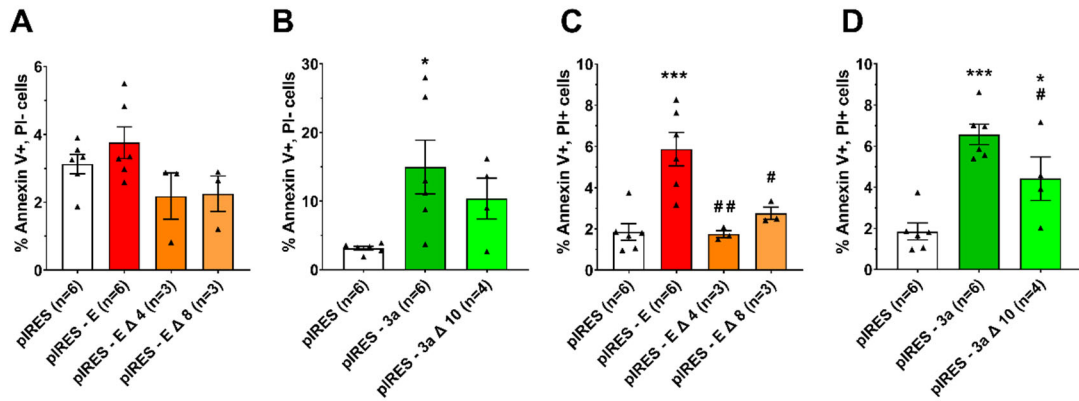
169 Both E and 3a proteins possess a C-terminal PDZ binding motif (PBM). E protein PBM has been  
170 suggested to be a virulence factor (11) and binds to host cells PDZ domains, leading to abnormal  
171 cellular distribution of the targeted proteins (31). 3a PBM interacts with at least five human PDZ-  
172 containing proteins (TJP1, NHERF3 & 4, RGS3, PARD3B), suggesting that it also alters cellular  
173 organization (32). We thus evaluated whether deletion of these domains impacts E and 3a  
174 proteins propensity to trigger cell death. Two C-terminal deletions used in previous studies to  
175 remove E protein PBM,  $\Delta 4$  for the last 4 amino-acids (31) and  $\Delta 8$  for the last 8 residues (11)  
176 abolished the pro-apoptotic effect of E protein (Figure 2). When looking individually at early and  
177 late cell death, we observed that both truncation of E and 3a protein decreased late cell death  
178 (suppl. Figure 2).





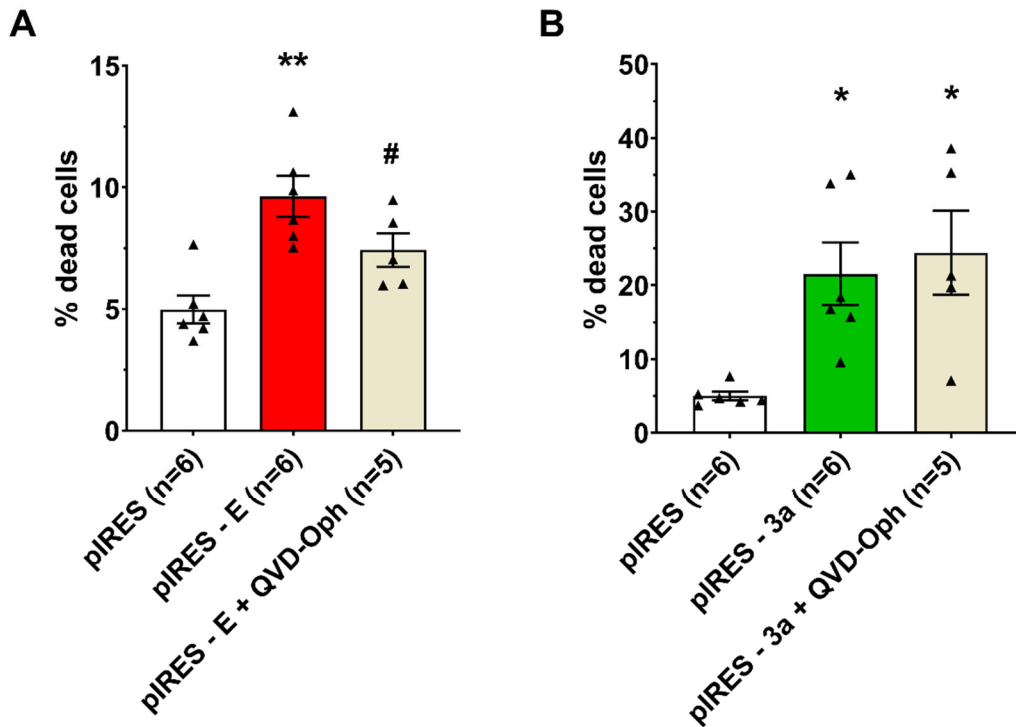
179

180 **Figure 2: Expression of E and 3a protein induces cell death.** (A) Flow cytometric analysis of  
 181 eGFP-positive CHO cells expressing only eGFP (pIRES), or co-expressing eGFP and one of the  
 182 following SARS-CoV-2 cDNA: the full-length E protein (pIRES - E), C-terminally deleted E protein  
 183 (pIRES - E Δ 4 or pIRES - E Δ 8), the full length 3a protein (pIRES - 3a) or the C-terminally deleted  
 184 3a protein (pIRES - 3a Δ 10). After 48 h of expression, cells were stained with annexin V  
 185 AlexaFluor 647 (APC)/propidium iodide (PI, Perc-P). (B) Mean ± sem of the percentage of  
 186 Annexin V+ cells among eGFP-positive CHO cells expressing only eGFP (pIRES), or eGFP and full-  
 187 length or truncated E protein. \*\*\* p<0.001 as compared to pIRES control, one-way ANOVA, ##  
 188 p<0.01 as compared to E protein, t-test. (C) Mean ± sem of the percentage of Annexin V+ cells  
 189 among eGFP-positive CHO cells expressing only eGFP (pIRES), or eGFP and full-length or  
 190 truncated 3a protein. \*\* p<0.01 as compared to pIRES control, one-way ANOVA.



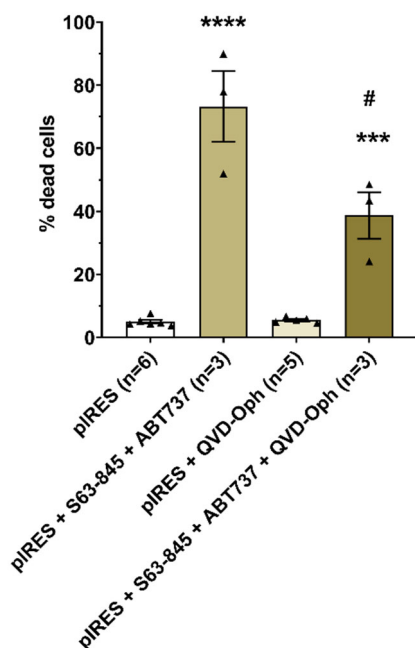
191  
192  
193  
194  
195  
196

**Suppl. Figure 2: Effects of E and 3a protein expression on early (Annexin V+, PI- in A&B) and late (Annexin V+, PI+ in C&D) cell death.** Mean  $\pm$  sem of the percentage of stained cells among eGFP-positive CHO cells expressing only eGFP (pIRES), or eGFP and full-length or truncated E or 3a protein. \*  $p < 0.05$ , \*\*\*  $p < 0.001$  as compared to pIRES control, one-way ANOVA, ##  $p < 0.01$ , #  $p < 0.05$  as compared to full length protein, t-test.



197  
198  
199  
200  
201  
202  
203

**Suppl. Figure 3: Caspase dependence of E and 3a protein-induced cell death.** (A) Cell death induced by E protein expression is reduced by the pan-caspase inhibitor QVD-Oph. \*\*  $p < 0.01$ , as compared to pIRES control, one-way ANOVA. #  $p < 0.05$  as compared to E protein, t-test. (B) Cell death induced by 3a protein expression is not reduced by the pan-caspase inhibitor QVD-Oph. \*  $p < 0.05$ , as compared to pIRES control, one-way ANOVA. Concentrations are indicated in the method section.



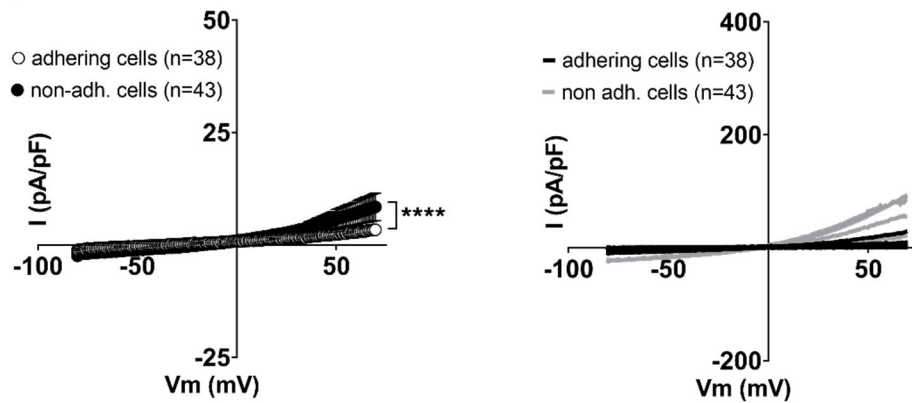
204

205 **Suppl. Figure 4: Test of the apoptosis inducers and inhibitor in CHO cells.** \*\*\*\* p<0.0001, \*\*\*  
 206 p<0.001, as compared to pIRES control, one-way ANOVA, # p<0.05 as compared to pIRES+S63-  
 207 845+ABT737, t-test.

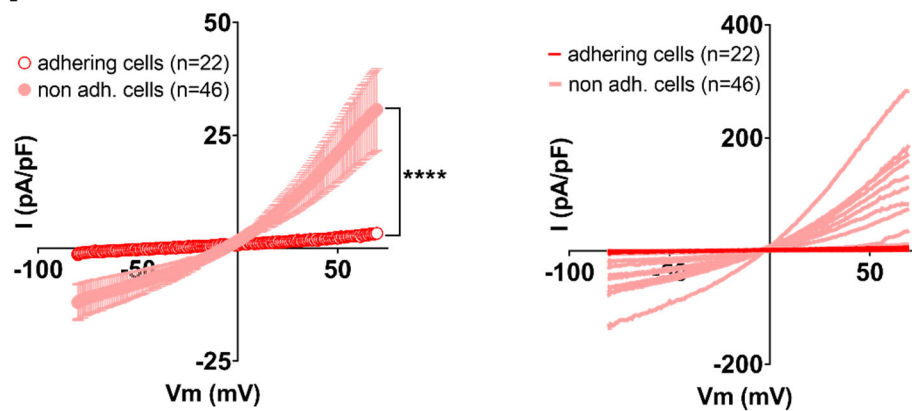
208 Since both E and 3a proteins promote cell death, we hypothesized that the cells starting to come  
 209 off the surface may express currents induced by cell death such as pannexin currents (24,25,33).  
 210 We thus compared patch-clamp recordings of adhering cells vs. non-adhering cells in the 3  
 211 conditions: control pIRES, pIRES - E and pIRES - 3a plasmids (Figure 3). In the control pIRES  
 212 condition, focusing on non-adhering cells in the 35-mm dish and using the ramp protocol, we  
 213 observed an outwardly rectifying current with a mean current density of  $8.5 \pm 3.1$  pA/pF at +70  
 214 mV, slightly higher than in spindle- or round-shaped adhering cells ( $3.4 \pm 0.8$  pA/pF). On the  
 215 other hand, in non-adhering cells expressing either the E or 3a protein, currents were much  
 216 larger in the E protein condition ( $I_{+70mV} = 31 \pm 9$  pA/pF, two-way ANOVA test on the ramp-evoked  
 217 currents: p<0.0001), but also in the 3a protein condition ( $I_{+70mV} = 44 \pm 13$  pA/pF, two-way ANOVA  
 218 test on the ramp-evoked currents: p<0.0001), as compared to non-adhering cells in the control  
 219 pIRES condition. Noteworthy, only a fraction of the cells was exhibiting large rectifying currents,  
 220 as shown in Figure 3: 4 out of 43 in the control pIRES condition, 14 out of 46 in the E protein  
 221 condition and 16 out of 41 in the 3a protein condition. These experiments suggest that cell death  
 222 and/or change in morphology induced by expression of E and 3a proteins may lead to an  
 223 increased membrane permeability by enhancing the expression or activity of an endogenous ion  
 224 channel.

225 The outwardly rectifying currents that we observed resemble apoptosis-induced and stretch-  
 226 induced pannexin currents (23–25). Thus, we applied the pannexin inhibitor carbenoxolone  
 227 (CBX) on non-adhering cells that display large outwardly rectifying currents (Figure 4). We  
 228 observed that CBX, applied at 50  $\mu$ mol/L, inhibits the observed current, restoring current  
 229 amplitudes similar to the ones observed in the control cells. Altogether, these observations  
 230 suggest that the current triggered by the expression of E and 3a protein is a pannexin current.

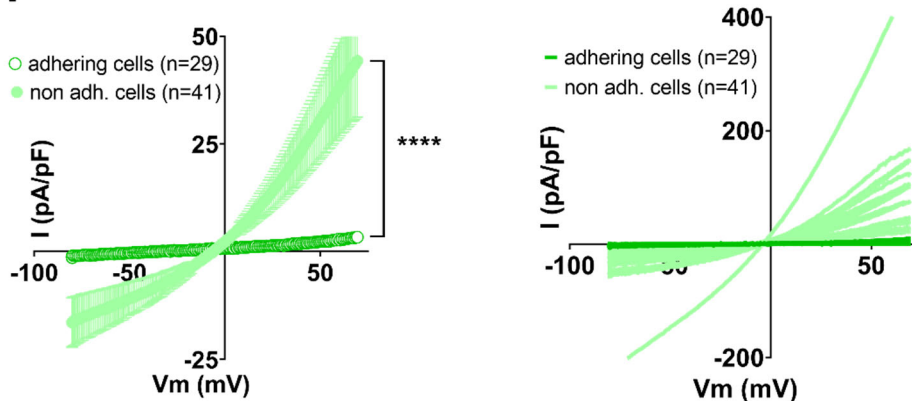
## A pIRES



## B pIRES - E

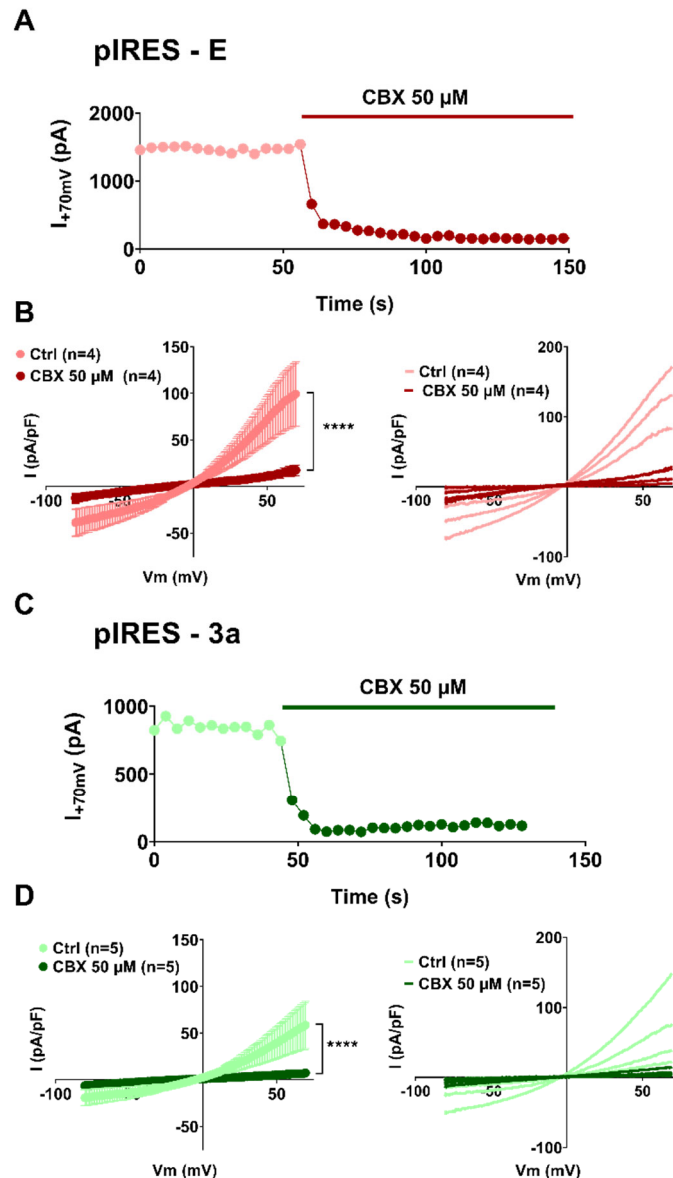


## C pIRES - 3a



231

232 **Figure 3. Expression of E and 3a protein is accompanied by outwardly rectifying currents in**  
 233 **non-adhering CHO cells only.** Left, average current densities ( $\pm$  sem) recorded during the ramp  
 234 protocol in adhering (empty circles) or non-adhering (filled circles) CHO cells expressing either  
 235 eGFP (A, pIRES), SARS-CoV-2 E and eGFP proteins (B, pIRES - E) or SARS-CoV-2 3a and eGFP  
 236 proteins (C, pIRES - 3a). Right, plot of the individual adhering cells (darker color) or non-adhering  
 237 cells (lighter color). \*\*\*\*  $p < 0.0001$ , as compared to adhering cells, two-way ANOVA.

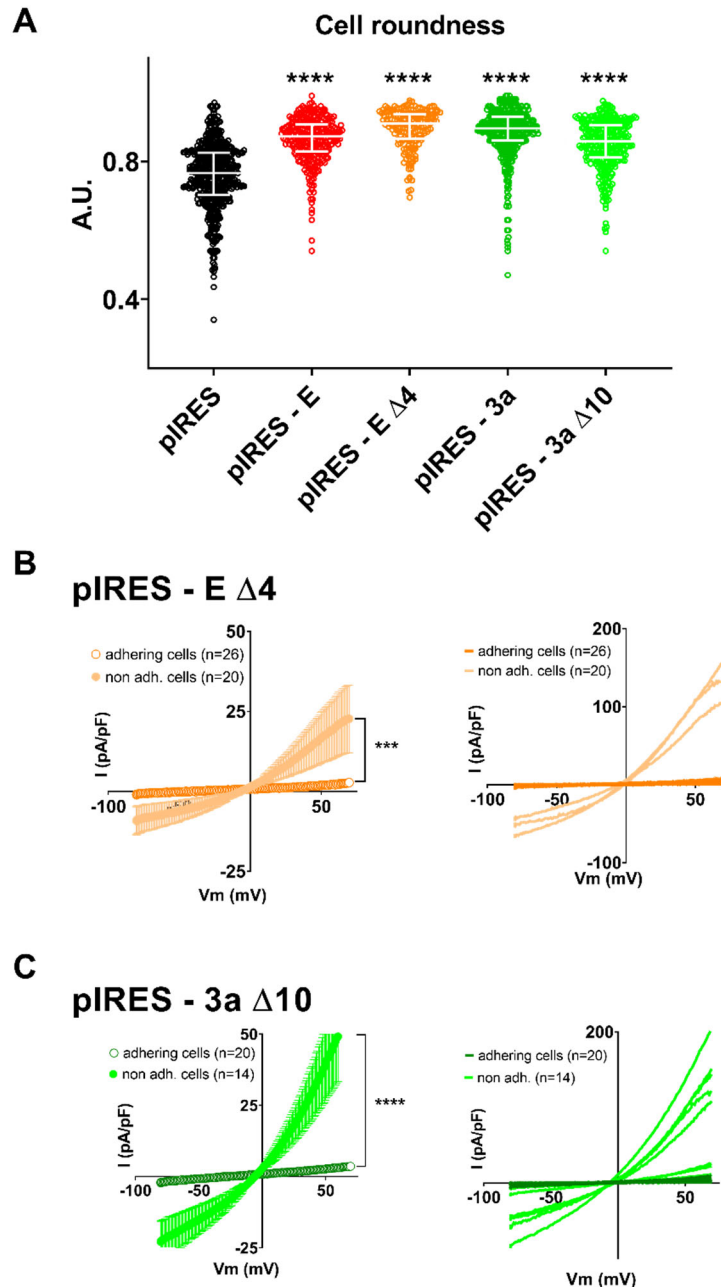


238

239 **Figure 4. Currents due to E and 3a protein expression in non-adhering CHO cells are suppressed**  
 240 **by the pannexin inhibitor carbenoxolone (CBX).** (A) Recording of the current amplitude in a  
 241 CHO cell expressing SARS-CoV-2 E and eGFP proteins that displays large outwardly rectifying  
 242 currents, in absence and presence of CBX. (B) Left, average current densities recorded during  
 243 the ramp protocol in non-adhering CHO cells, expressing SARS-CoV-2 E and eGFP proteins (pIRES  
 244 - E), in absence (Ctrl, lighter color) and presence of CBX (darker color). Right, plot of the  
 245 individual non-adhering cells in absence (lighter color) and presence of CBX (darker color). (C)  
 246 Recording of the current amplitude in a CHO cell expressing SARS-CoV-2 3a and eGFP proteins  
 247 that displays the outwardly rectifying currents, in absence and presence of CBX. (D) Left,  
 248 average current densities recorded during the ramp protocol in non-adhering CHO cells, expressing  
 249 SARS-CoV-2 3a and eGFP proteins (pIRES - E), in absence (Ctrl, lighter color) and presence of CBX  
 250 (darker color). Right, plot of the individual non-adhering cells in absence (lighter color) and  
 251 presence of CBX (darker color). \*\*\*  $p < 0.001$  or \*\*\*\*  $p < 0.0001$ , as compared to Ctrl, two-way  
 252 ANOVA with repeated measures.

253 We reported above (Figure 2) that deleting the last 4 amino-acids of E protein ( $\Delta 4$ ) drastically  
254 reduced its pro-apoptotic effect. Cells expressing the  $\Delta 4$  E protein showed an average roundness  
255 similar to cells expressing the WT protein, suggesting that deletion did not prevent its effect on  
256 cell morphology (Figure 5A and suppl. Figure 5). Also, when focusing on round and non-adhering  
257  $\Delta 4$  E protein expressing cells, we could still record large outwardly rectifying currents (5 out of  
258 20 cells), suggesting that C-terminal deletion of E protein does not abolish the induction of  
259 pannexin currents, despite prevention of apoptosis probed by flow cytometry experiments  
260 (Figure 5B).

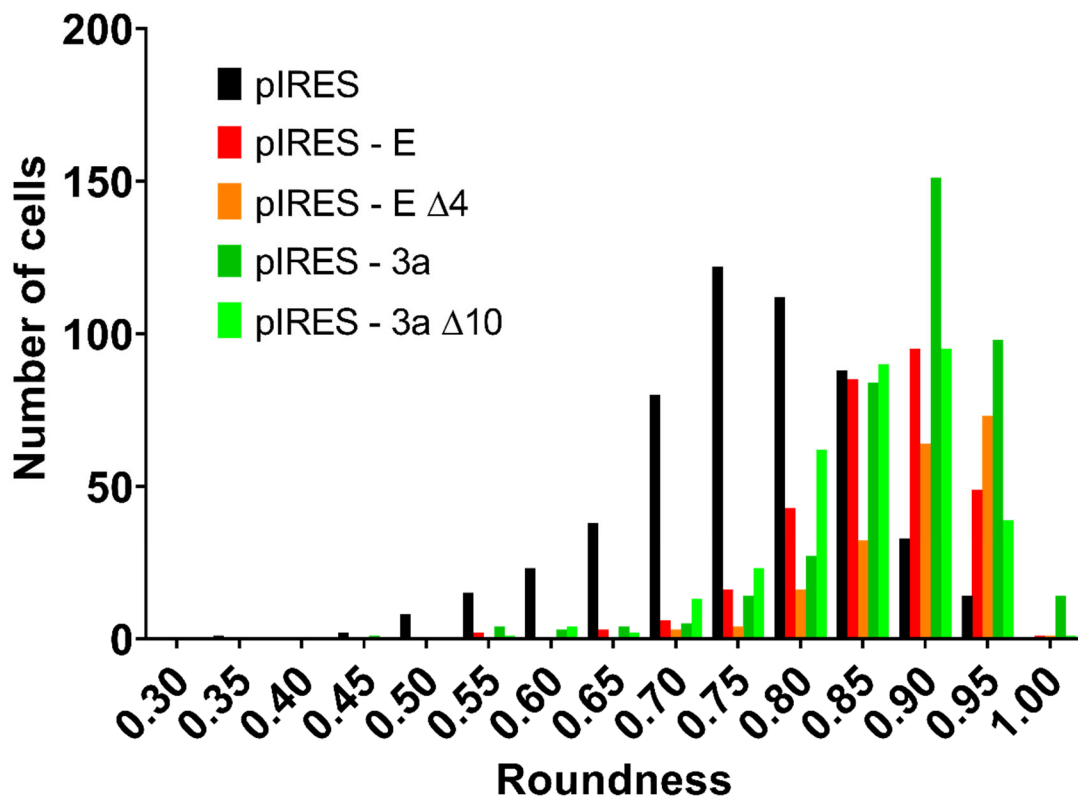
261 We also reported in Figure 2 that the deletion of the last 10 amino-acids of 3a protein ( $\Delta 10$ ) also  
262 decreased cell death albeit to a lesser extent. As for E protein deletion, cells expressing the  
263 truncated 3a protein showed an average roundness similar to cells expressing the WT protein  
264 (Figure 5A and suppl. Figure 5). Focusing on the non-adhering cells, we could still record large  
265 outwardly rectifying currents (9 out of 14 cells), suggesting that deletion of the last 10 amino-  
266 acids is not sufficient to completely abolish the induction of pannexin-like currents (Figure 5C).



267

268 **Figure 5. C-terminal deletion of E and 3a protein does not prevent cell characteristic changes.**

269 **(A)** Cell roundness measured in CHO cells expressing eGFP (pIRES) alone, or in combination with  
 270 WT (pIRES - E) or the C-terminally deleted E protein (pIRES - E  $\Delta$ 4) or in combination with WT  
 271 (pIRES - 3a) or the C-terminally deleted 3a protein (pIRES - 3a  $\Delta$ 10). Plot of individual cells,  
 272 median  $\pm$  interquartile range. \*\*\*\*  $p < 0.0001$  as compared to pIRES control, Kruskal-Wallis test.  
 273 **(B)** Left, average current densities ( $\pm$  sem) recorded during the ramp protocol in adhering (empty circles) or non-adhering (filled circles) CHO cells expressing the C-terminally deleted E protein  
 274 (pIRES - E  $\Delta$ 4). Right, plot of the individual adhering (darker color) or non-adhering cells (lighter  
 275 color). \*\*\*  $p < 0.001$ , as compared to adhering cells, two-way ANOVA. **(C)** Left, average current  
 276 densities ( $\pm$  sem) recorded during the ramp protocol in adhering (empty circles) or non-adhering  
 277 (filled circles) CHO cells expressing the C-terminally deleted 3a protein (pIRES - 3a  $\Delta$ 10). Right,  
 278 plot of the individual adhering (darker color) or non-adhering cells (lighter color). \*\*\*\*  $p < 0.0001$ ,  
 279 as compared to adhering cells, two-way ANOVA.  
 280



281  
 282 **Suppl. Figure 5.** Distribution of cells roundness from the analysis of 5 areas of 1.7 mm x 1.7 mm  
 283 of transfected CHO cells (Cf. Figure 5A).

284 **Discussion**

285 The concept that SARS-CoV E or 3a proteins could be viroporins expressed at the plasma  
 286 membrane is a seducing one as it could help the identification of new therapeutic drugs against  
 287 COVID-19 by setting up a screening program on the channel activity. However, this concept was  
 288 controversial and part of the reasons that explain the controversy about the function of E and  
 289 3a proteins is likely linked to the fact that these proteins also trigger morphological alterations  
 290 and cell death. Cell death is associated to important changes in lipid composition and membrane  
 291 permeability which suffices to fuel the controversy. One could imagine for instance that cell  
 292 death would be a way to activate the function of E and 3a proteins at the plasma membrane,  
 293 but an alternative hypothesis could be simply that cell death triggers an endogenous cell  
 294 conductance unrelated to the cell function of E and 3a viral proteins. The only way to address  
 295 these issues was to confirm the cell toxicity, to characterize the impact of the expression of these  
 296 proteins on cell shape and behavior, to measure plasma membrane conductance, and to  
 297 characterize them to get an idea of their nature and probe a pharmacological agent that would  
 298 match the conductance identity. We manage to solve these issues by carefully characterizing  
 299 the membrane conductances triggered by both E and 3a proteins. The fact that both proteins  
 300 trigger the same conductance independently of each other was a first indication that they could  
 301 not be viroporins at the plasma membrane. The second hint was that adhering cells, whether  
 302 they had a round-shape or not, did not exhibit any outward conductance in spite of E or 3a  
 303 protein expression. Finally, the sensitivity to carbenoxolone of the outward currents triggered  
 304 by E or 3a proteins in non-adhering cells was an indication that these viral proteins trigger  
 305 cellular alterations, such as morphological changes and cell death that are inducers of pannexin-



306 like current. Globally, these observations remain consistent with previous observations that  
307 both E and 3a proteins are mainly localized in intracellular compartments in various cell types  
308 (14,34–38). Therefore, it is fair to mention that we cannot fully conclude on the viroporin nature  
309 of these viral proteins as their localization in subcellular organelles prevents us for clearly testing  
310 their intrinsic potential for channel activity.

311 We showed that expression of either of these two proteins in CHO cells induces an increase in  
312 cell death, as quantified by flow cytometry experiments. It is likely, although we did not  
313 investigate this point in details, that this cell death accompanies the change in cell morphology  
314 and Petri dish detachment. As such, our observation that pannexin-like currents are mainly  
315 observed in detached round-shaped cells indicates that major cell morphology changes, up to  
316 level of surface detachment, is required for the induction of pannexin-like currents. Whatever  
317 the exact mechanism, the upregulation of pannexin channels upon cell death was already  
318 observed earlier (39). It is thus not so surprising in fact that other reports faced problems  
319 reporting and identifying the conductances triggered by E and 3a viral proteins. The conditions  
320 for observing them are indeed quite drastic and require examining cells that are in the combined  
321 dying and detachment process, something that is not naturally pursued by researchers,  
322 especially if one hopes to detect a viroporin activity. To reconcile our data with earlier  
323 publications, we noticed that whole-cell currents observed by others after SARS-CoV-1 E or 3a  
324 protein expression in HEK 293 cells (13,17) were also very similar to pannexin currents:  
325 outwardly rectifying current, with a reversal potential close to 0 mV at physiological ion  
326 concentrations indicating a poor ion selectivity, and amplitude of a few 100 pA.

327 One possibility is that the pannexin-like currents that we observed are due to the classical  
328 caspase-induced cleavage of pannexin (40). Intriguingly, deletion of the C-terminal PBM of E  
329 protein abolished its pro-apoptotic effect but cell morphology alteration and pannexin-like  
330 currents were still present. Regarding the 3a protein, deletion of its PBM domain only decreased  
331 and did not completely abolish the promoted cell death, but again cell morphology alteration  
332 and pannexin-like currents were preserved. Altogether, these results suggest that cell  
333 morphology modification and pannexin induction may be linked and these processes are not  
334 necessarily accompanied by cell death. One has to keep in mind that pannexin currents are  
335 activated by many stimuli in addition to cell death (40). In particular, pannexin currents are also  
336 stretch-activated and may be enhanced in the detached cells which are undergoing major  
337 morphological alterations (23). If pannexins are already activated by stretch, they would not be  
338 overactivated by their cleavage by caspase, which would explain the fact that E and 3a proteins  
339 truncation do not prevent pannexin current, but only cell death.

340 In conclusion, SARS-CoV-2 native E and 3a proteins, and probably SARS-CoV-1 ones, do not act  
341 as plasma membrane ion channels, but trigger the activity of plasma membrane pannexin  
342 channels, most likely through morphological alteration of the cells. However, our study does not  
343 rule out potential channel activity in intracellular membranes leading to cell death. Future  
344 studies will give more insights on the role of pannexin channels in COVID-19 physiopathology  
345 and treatment (41–43).

## 346 **Materials and Methods**

### 347 *Cell culture*

348 The Chinese Hamster Ovary cell line, CHO, was obtained from the American Type Culture  
349 Collection (CRL-11965) and cultured in Dulbecco's modified Eagle's medium (Gibco 41966-029,

350 USA) supplemented with 10% fetal calf serum (Eurobio, EU), 2 mM L-Glutamine and antibiotics  
351 (100 U/mL penicillin and 100 µg/mL streptomycin, Corning, EU) at 5% CO<sub>2</sub>, maintained at 37°C  
352 in a humidified incubator. This cell line was confirmed to be mycoplasma-free (MycoAlert,  
353 Lonza).

#### 354 *Drugs*

355 Carbenoxolone disodium salt was purchased from Sigma and 100 mmol/L stock solution was  
356 prepared in H<sub>2</sub>O. Drugs used for flow cytometry experiments were QVD-Oph (#OPH001, R&D  
357 Systems, 10 mmol/L stock solution in DMSO), S63-845 (Chemieteck, 10 mmol/L stock solution  
358 in DMSO), ABT737 (Selleckchem, 10 mmol/L stock solution in DMSO).

#### 359 *Construction of E and 3a proteins encoding plasmids*

360 SARS-CoV-2 E and 3a nucleotide sequences, containing a Kozak sequence added right before the  
361 ATG (RefSeq NC\_045512.2) were synthesized by Eurofins (Ebersberg, EU) and subcloned into  
362 the pIRES2 vector with eGFP in the second cassette (Takara Bio Europe, EU). Truncated Δ4 and  
363 Δ8 E proteins, as well as Δ10 3a protein constructs, lacking the last 12, 24 and 30 last nucleotides,  
364 respectively, were also synthesized by Eurofins. Plasmid cDNAs were systematically re-  
365 sequenced by Eurofins after each plasmid in-house midiprep (Qiagen, EU).

#### 366 *E and 3a cDNA transfection*

367 The Fugene 6 transfection reagent (Promega, WI, USA) was used to transfect WT and mutant E  
368 and 3a plasmids for patch-clamp, morphology analysis and flow cytometry experiments  
369 according to the manufacturer's protocol. Cells were cultured in 35-mm dishes and transfected,  
370 at a 20% confluence for patch clamp experiments and 50% confluence for flow cytometry assay,  
371 with a pIRES plasmid (2 µg DNA) with the first cassette empty or containing wild-type or  
372 truncated SARS-CoV-2 E or 3a protein sequence. For morphology analysis, cells were cultured in  
373 ibidi µ-Slide 8 well dishes and transfected at a 20% confluence with the same plasmids. In  
374 pIRES2-eGFP plasmids, the second cassette (eGFP) is less expressed than the first cassette,  
375 guaranteeing expression of high level of the protein of interest in fluorescent cells (28,29).

#### 376 *Electrophysiology*

377 Two days after transfection, CHO cells were mounted on the stage of an inverted microscope  
378 and bathed with a Tyrode solution (in mmol/L: NaCl 145, KCl 4, MgCl<sub>2</sub> 1, CaCl<sub>2</sub> 1, HEPES 5, glucose  
379 5, pH adjusted to 7.4 with NaOH) maintained at 22.0 ± 2.0°C. Patch pipettes (tip resistance: 2.0  
380 to 2.5 MΩ) were pulled from soda-lime glass capillaries (Kimble-Chase, USA) with a Sutter P-30  
381 puller (USA). A fluorescent cell was selected by epifluorescence. The pipette was filled with  
382 intracellular medium containing (in mmol/L): KCl, 100; Kgluconate, 45; MgCl<sub>2</sub>, 1; EGTA, 5; HEPES,  
383 10; pH adjusted to 7.2 with KOH. Stimulation and data recording were performed with pClamp  
384 10, an A/D converter (Digidata 1440A) and a Multiclamp 700B (all Molecular Devices) or a VE-2  
385 patch-clamp amplifier (Alembic Instruments). Currents were acquired in the whole-cell  
386 configuration, low-pass filtered at 10 kHz and recorded at a sampling rate of 50 kHz. First, series  
387 of twenty 30-ms steps to -80 mV were applied from holding potential (HP) of alternatively -70  
388 mV and -90 mV to subsequently off-line calculate C<sub>m</sub> and R<sub>s</sub> values from the recorded currents.  
389 Currents were then recorded using a 1-s ramp protocol from -80 mV to +70 mV, every 4 s (cf.  
390 Figure 1). Regarding non-adhering cells, we considered them as with large current density when  
391 the current density measured at +70 mV was superior to mean + 2 x standard deviation of the  
392 current density in adhering cells, in the same condition.

393 *Cell morphology assay*

394 Cell roundness was estimated using the *Analyze Particle* function of the Fiji software, as  
395 described in suppl. Figure 1.

396 *Flow cytometry assay*

397 Two days after transfection, CHO cells were prepared to cell death detection following the user  
398 guide (<https://assets.thermofisher.com/TFS-Assets/LSG/manuals/mp13199.pdf>), to measure  
399 annexin V binding and propidium iodide (PI) intake. The cells were washed with cold PBS,  
400 trypsinized, collected by centrifugation and gently resuspended in annexin-binding buffer  
401 (V13246, Invitrogen, USA) at  $1 \times 10^6$  cells/mL. To each 300- $\mu$ L cell suspension were added 0.5  $\mu$ L  
402 of annexin V AlexaFluor 647 (A23204, Invitrogen) and 1  $\mu$ L of propidium iodide (PI) at 100  $\mu$ g/mL  
403 (P3566, Invitrogen). CHO cells were incubated at room temperature for 15 minutes in the dark,  
404 and then maintained on ice until flow cytometry analysis within one hour.

405 To study the cell death pathways induced by E and 3a protein expression, non-transfected or  
406 transfected CHO cells were treated with inhibitors or inducers of apoptosis (inhibitor: 5  $\mu$ mol/L  
407 QVD-OPh incubated for 48 h; activators: 3  $\mu$ mol/L S63-845 + 8  $\mu$ mol/L ABT737 incubated for 3  
408 h).

409 The cytometer BD FACSCanto (BD Biosciences, USA) was used to sample acquisition. CHO cells  
410 transfected with an empty plasmid were used to determine the population to be analyzed.  
411 Monolabeled cells were used to establish the photomultiplier voltage of each channel (PMT)  
412 and to proceed with fluorescence compensation after the acquisitions. In order to detect cell  
413 death, only eGFP-positive CHO cells (FITC) were analyzed to Annexin V AlexaFluor 647 (APC) and  
414 PI (Perc-P) labeling. Analyses were performed using FlowJo software.

415 **Acknowledgements**

416 We thank the Agence Nationale de la Recherche for its financial support to the Région Pays de  
417 la Loire (ANR FLASH Covid-19 - CoV2-E-TARGET) and the laboratory of excellence 'Ion Channels,  
418 Science and Therapeutics' (grant No. ANR-11-LABX-0015). We acknowledge the IBISA  
419 MicroPICell facility (Biogenouest), member of the national infrastructure France-Bioimaging  
420 supported by the French national research agency (ANR-10-INBS-04). We thank the Cytometry  
421 Facility Cytocell from Nantes for expert technical assistance. We thank Hugues Abriel and Jean-  
422 Sebastien Rougier (Institute of Biochemistry and Molecular Medicine, university of Bern) for  
423 fruitful discussions and support and critical reading of the manuscript.

## 424 **References**

- 425 1. Drosten C, Günther S, Preiser W, van der Werf S, Brodt HR, Becker S, et al. Identification of  
426 a Novel Coronavirus in Patients with Severe Acute Respiratory Syndrome. *N Engl J Med*. 15  
427 mai 2003;348(20):1967-76.
- 428 2. Zaki AM, van Boheemen S, Bestebroer TM, Osterhaus ADME, Fouchier RAM. Isolation of a  
429 Novel Coronavirus from a Man with Pneumonia in Saudi Arabia. *N Engl J Med*. 8 nov  
430 2012;367(19):1814-20.
- 431 3. Burki T. The future of Paxlovid for COVID-19. *The Lancet Respiratory Medicine*. juill  
432 2022;10(7):e68.
- 433 4. Ledford H. Hundreds of COVID trials could provide a deluge of new drugs. *Nature*. 3 mars  
434 2022;603(7899):25-7.
- 435 5. Ison MG. Antivirals and resistance: influenza virus. *Current Opinion in Virology*. déc  
436 2011;1(6):563-73.
- 437 6. Wilson L, Mckinlay C, Gage P, Ewart G. SARS coronavirus E protein forms cation-selective  
438 ion channels. *Virology*. déc 2004;330(1):322-31.
- 439 7. Wilson L, Gage P, Ewart G. Hexamethylene amiloride blocks E protein ion channels and  
440 inhibits coronavirus replication. *Virology*. sept 2006;353(2):294-306.
- 441 8. Torres J, Maheswari U, Parthasarathy K, Ng L, Liu DX, Gong X. Conductance and  
442 amantadine binding of a pore formed by a lysine-flanked transmembrane domain of SARS  
443 coronavirus envelope protein. *Protein Sci*. sept 2007;16(9):2065-71.
- 444 9. Verdiá-Báguena C, Nieto-Torres JL, Alcaraz A, DeDiego ML, Torres J, Aguilera VM, et al.  
445 Coronavirus E protein forms ion channels with functionally and structurally-involved  
446 membrane lipids. *Virology*. oct 2012;432(2):485-94.
- 447 10. Nieto-Torres JL, Verdiá-Báguena C, Jimenez-Guardeño JM, Regla-Nava JA, Castaño-  
448 Rodríguez C, Fernandez-Delgado R, et al. Severe acute respiratory syndrome coronavirus E  
449 protein transports calcium ions and activates the NLRP3 inflammasome. *Virology*. nov  
450 2015;485:330-9.
- 451 11. Castaño-Rodríguez C, Honrubia JM, Gutiérrez-Álvarez J, DeDiego ML, Nieto-Torres JL,  
452 Jimenez-Guardeño JM, et al. Role of Severe Acute Respiratory Syndrome Coronavirus  
453 Viroporins E, 3a, and 8a in Replication and Pathogenesis. Denison MR, éditeur. *mBio*. 5 juill  
454 2018;9(3):e02325-17.
- 455 12. McClenaghan C, Hanson A, Lee SJ, Nichols CG. Coronavirus Proteins as Ion Channels:  
456 Current and Potential Research. *Front Immunol*. 9 oct 2020;11:573339.
- 457 13. Pervushin K, Tan E, Parthasarathy K, Lin X, Jiang FL, Yu D, et al. Structure and Inhibition of  
458 the SARS Coronavirus Envelope Protein Ion Channel. Baric RS, éditeur. *PLoS Pathog*. 10 juill  
459 2009;5(7):e1000511.
- 460 14. Nieto-Torres JL, DeDiego ML, Álvarez E, Jiménez-Guardeño JM, Regla-Nava JA, Llorente M,  
461 et al. Subcellular location and topology of severe acute respiratory syndrome coronavirus  
462 envelope protein. *Virology*. juill 2011;415(2):69-82.

- 463 15. Cabrera-Garcia D, Bekdash R, Abbott GW, Yazawa M, Harrison NL. The envelope protein of  
464 SARS-CoV-2 increases intra-Golgi pH and forms a cation channel that is regulated by pH. *J*  
465 *Physiol.* juin 2021;599(11):2851-68.
- 466 16. Breitingner U, Farag NS, Sticht H, Breitingner HG. Viroporins: Structure, function, and their  
467 role in the life cycle of SARS-CoV-2. *The International Journal of Biochemistry & Cell*  
468 *Biology.* avr 2022;145:106185.
- 469 17. Chan CM, Tsoi H, Chan WM, Zhai S, Wong CO, Yao X, et al. The ion channel activity of the  
470 SARS-coronavirus 3a protein is linked to its pro-apoptotic function. *The International*  
471 *Journal of Biochemistry & Cell Biology.* nov 2009;41(11):2232-9.
- 472 18. Lu W, Zheng BJ, Xu K, Schwarz W, Du L, Wong CKL, et al. Severe acute respiratory  
473 syndrome-associated coronavirus 3a protein forms an ion channel and modulates virus  
474 release. *Proc Natl Acad Sci USA.* 15 août 2006;103(33):12540-5.
- 475 19. Schwarz S, Wang K, Yu W, Sun B, Schwarz W. Emodin inhibits current through SARS-  
476 associated coronavirus 3a protein. *Antiviral Research.* avr 2011;90(1):64-9.
- 477 20. Schwarz S, Sauter D, Wang K, Zhang R, Sun B, Karioti A, et al. Kaempferol Derivatives as  
478 Antiviral Drugs against the 3a Channel Protein of Coronavirus. *Planta Med.* 23 janv  
479 2014;80(02/03):177-82.
- 480 21. Ren Y, Shu T, Wu D, Mu J, Wang C, Huang M, et al. The ORF3a protein of SARS-CoV-2  
481 induces apoptosis in cells. *Cell Mol Immunol.* août 2020;17(8):881-3.
- 482 22. Xia B, Shen X, He Y, Pan X, Liu FL, Wang Y, et al. SARS-CoV-2 envelope protein causes acute  
483 respiratory distress syndrome (ARDS)-like pathological damages and constitutes an  
484 antiviral target. *Cell Res.* août 2021;31(8):847-60.
- 485 23. Bao L, Locovei S, Dahl G. Pannexin membrane channels are mechanosensitive conduits for  
486 ATP. *FEBS Letters.* 13 août 2004;572(1-3):65-8.
- 487 24. Senthivinayagam S, Serbulea V, Upchurch CM, Polanowska-Grabowska R, Mendu SK, Sahu  
488 S, et al. Adaptive thermogenesis in brown adipose tissue involves activation of pannexin-1  
489 channels. *Molecular Metabolism.* févr 2021;44:101130.
- 490 25. Bhat EA, Sajjad N. Human Pannexin 1 channel: Insight in structure–function mechanism  
491 and its potential physiological roles. *Mol Cell Biochem.* mars 2021;476(3):1529-40.
- 492 26. Uchida K, Emoto K, Daleke DL, Inoue K, Umeda M. Induction of Apoptosis by  
493 Phosphatidylserine. *Journal of Biochemistry.* 1 juin 1998;123(6):1073-8.
- 494 27. Crea F, Sarti D, Falciani F, Al-Rubeai M. Over-expression of hTERT in CHO K1 results in  
495 decreased apoptosis and reduced serum dependency. *Journal of Biotechnology.* janv  
496 2006;121(2):109-23.
- 497 28. Mizuguchi H, Xu Z, Ishii-Watabe A, Uchida E, Hayakawa T. IRES-Dependent Second Gene  
498 Expression Is Significantly Lower Than Cap-Dependent First Gene Expression in a  
499 Bicistronic Vector. *Molecular Therapy.* avr 2000;1(4):376-82.

- 500 29. Choveau FS, Rodriguez N, Ali FA, Labro AJ, Rose T, Dahimène S, et al. KCNQ1 Channels  
501 Voltage Dependence through a Voltage-dependent Binding of the S4-S5 Linker to the Pore  
502 Domain. *Journal of Biological Chemistry*. janv 2011;286(1):707-16.
- 503 30. Yu SP, Kerchner GA. Endogenous voltage-gated potassium channels in human embryonic  
504 kidney (HEK293) cells. *J Neurosci Res*. 1 juin 1998;52(5):612-7.
- 505 31. Teoh KT, Siu YL, Chan WL, Schlüter MA, Liu CJ, Peiris JSM, et al. The SARS Coronavirus E  
506 Protein Interacts with PALS1 and Alters Tight Junction Formation and Epithelial  
507 Morphogenesis. Nusrat A, éditeur. *MBoC*. 15 nov 2010;21(22):3838-52.
- 508 32. Caillet-Saguy C, Durbesson F, Rezelj VV, Gogl G, Tran QD, Twizere J, et al. Host PDZ-  
509 containing proteins targeted by SARS-CoV-2. *FEBS J*. sept 2021;288(17):5148-62.
- 510 33. Poon IKH, Chiu YH, Armstrong AJ, Kinchen JM, Juncadella IJ, Bayliss DA, et al. Unexpected  
511 link between an antibiotic, pannexin channels and apoptosis. *Nature*. 20 mars  
512 2014;507(7492):329-34.
- 513 34. Yuan X, Li J, Shan Y, Yang Z, Zhao Z, Chen B, et al. Subcellular localization and membrane  
514 association of SARS-CoV 3a protein. *Virus Research*. mai 2005;109(2):191-202.
- 515 35. Nal B, Chan C, Kien F, Siu L, Tse J, Chu K, et al. Differential maturation and subcellular  
516 localization of severe acute respiratory syndrome coronavirus surface proteins S, M and E.  
517 *Journal of General Virology*. 1 mai 2005;86(5):1423-34.
- 518 36. Liao Y, Yuan Q, Torres J, Tam JP, Liu DX. Biochemical and functional characterization of the  
519 membrane association and membrane permeabilizing activity of the severe acute  
520 respiratory syndrome coronavirus envelope protein. *Virology*. juin 2006;349(2):264-75.
- 521 37. Cohen JR, Lin LD, Machamer CE. Identification of a Golgi Complex-Targeting Signal in the  
522 Cytoplasmic Tail of the Severe Acute Respiratory Syndrome Coronavirus Envelope Protein.  
523 *J Virol*. 15 juin 2011;85(12):5794-803.
- 524 38. Kern DM, Sorum B, Mali SS, Hoel CM, Sridharan S, Remis JP, et al. Cryo-EM structure of  
525 SARS-CoV-2 ORF3a in lipid nanodiscs. *Nat Struct Mol Biol*. juill 2021;28(7):573-82.
- 526 39. Chekeni FB, Elliott MR, Sandilos JK, Walk SF, Kinchen JM, Lazarowski ER, et al. Pannexin 1  
527 channels mediate 'find-me' signal release and membrane permeability during apoptosis.  
528 *Nature*. oct 2010;467(7317):863-7.
- 529 40. Navis KE, Fan CY, Trang T, Thompson RJ, Derksen DJ. Pannexin 1 Channels as a Therapeutic  
530 Target: Structure, Inhibition, and Outlook. *ACS Chem Neurosci*. 5 août  
531 2020;11(15):2163-72.
- 532 41. Swayne LA, Johnstone SR, Ng CS, Sanchez-Arias JC, Good ME, Penuela S, et al.  
533 Consideration of Pannexin 1 channels in COVID-19 pathology and treatment. *American  
534 Journal of Physiology-Lung Cellular and Molecular Physiology*. 1 juill 2020;319(1):L121-5.
- 535 42. Luu R, Valdebenito S, Scemes E, Cibelli A, Spray DC, Rovegno M, et al. Pannexin-1 channel  
536 opening is critical for COVID-19 pathogenesis. *iScience*. déc 2021;24(12):103478.

537 43. Nadeali Z, Mohammad-Rezaei F, Aria H, Nikpour P. Possible role of pannexin 1 channels  
538 and purinergic receptors in the pathogenesis and mechanism of action of SARS-CoV-2 and  
539 therapeutic potential of targeting them in COVID-19. *Life Sciences*. mai 2022;297:120482.

540